Catalysis Today 176 (2011) 56–62

Contents lists available at ScienceDirect

Catalysis Today

journal homepage: www.elsevier.com/locate/cattod

Impact of thermal and vehicle aging on the structure and functionalities of a lean NOx-trap

Sheïma Benramdhane[a], Claire-Noelle Millet[a], Eric Jeudy[a], Jacques Lavy[a,*], Vanessa Blasin Aubé[b], Marco Daturi[b]

[a] IFP Energies nouvelles, rond point de l'échangeur de Solaize, BP3, 69360 Solaize, France
[b] Laboratoire Catalyse et Spectrochimie, ENSICAEN, Université de Caen, CNRS, 6 Bd Maréchal Juin, F-14050 Caen, France

ARTICLE INFO

Article history:
Received 28 September 2010
Received in revised form 21 March 2011
Accepted 22 March 2011
Available online 6 July 2011

Keywords:
Lean NOx Trap (LNT)
NOx storage catalyst
Thermal aging
Vehicle aging
Sulfation
SO_2
Operando FTIR

ABSTRACT

Investigations of the aging behaviour of a commercial lean NOx trap (LNT) are reported in this paper. Two aging processes were tested and compared: a hydrothermal aging at 800 °C and a vehicle aging corresponding to a 80,000 km use. Samples were characterized with Operando FTIR, XRF, XRD, SEM-EDX, TEM, and BET analyses. LNT functionalities were evaluated using a flow reactor capable of performing NOx storage and conversion measurements, and correlated with the LNT structure evolution due to aging. The results highlighted that Pt sintering had an impact on the NO oxidation functionality and also deteriorated the Pt/Ba interface. It was hence partly responsible for the NSC decrease. Both aging processes had a similar impact on the LNT NOx storage capacity (NSC) although their structural evolutions were different: $BaAl_2O_4$ formation on the hydrothermal aged catalyst versus barium poisoned by sulphur on the vehicle aged catalyst.

1. Introduction

Emissions of nitrogen oxides (NOx) and particulate matter (PM) produced by Diesel-powered vehicles represent a major environmental and health issue in highly populated areas. A number of exhaust gas after treatment systems have been developed in recent years for Diesel engines such as the Diesel particulate filter (DPF) regarding PM abatement and the Lean NOx-Trap (LNT) or urea Selective Catalytic Reduction system (SCR) regarding NOx emission reduction from lean burn engine. LNTs achieve NOx conversion through successive cycles of lean and rich operating conditions [1]. The concept is based on the adsorption of NOx on a trapping material during long periods of excess oxygen followed by shorter periods with a lack of oxygen during which the stored NOx are released and reduced to mainly N_2, but also partly N_2O or NH_3. Reductants are mainly hydrocarbons issued from a specific fuel injection strategy into the cylinder or the exhaust pipe. Lean/rich transitions are managed by the engine control unit. Main components of the catalytic washcoat are usually alumina for the support, Pt, Pd and Rh as noble metals to provide oxidative and reductive functionalities, and a basic additive (often a barium salt) known for its high affinity for NOx as a storage component [2].

NOx traps also show some undesired reactivity in regards to sulphur compounds which are present in exhaust gases from both Diesel and gasoline engines [3–6]. SO_3 reacts with barium and alumina to form barium and aluminium sulphates which are more stable than the corresponding nitrates. This causes gradual saturation of the storage material with sulphur and loss of activity towards NOx storage [5]. Periodic desulfation (DeSOx) hence require higher temperatures which are detrimental to the life of the catalyst. For this reason, deactivation by sulphur and the corresponding thermal aging are key obstacles to a widespread implementation of the LNT [7–12].

The work described in this paper focuses on the impact of aging on the functionalities of a commercial lean NOx-trap. Two aging processes were tested and compared: a hydrothermal aging at 800 °C and a vehicle aging corresponding to a 80,000 km use and considered as a reference. Functionalities were evaluated on a Synthetic Gas Bench (SGB) and reactivity results were correlated with the analysis of the structural and chemical evolution of the catalyst. A FTIR *Operando* study allowed to further analyse the mechanisms occurring on the catalyst surface and to highlight the most critical points.

* Corresponding author. Tel.: +33 1 37702730; fax: +33 1 37702014.
E-mail addresses: jacques.lavy@ifpen.fr, sheima.benramdhane@ifpen.fr (J. Lavy).

0920-5861/$ – see front matter © 2011 Elsevier B.V. All rights reserved.
doi:10.1016/j.cattod.2011.03.049

2. Experimental

2.1. Catalyst

The commercial NOx trap that was investigated in this study was supplied by RENAULT. It has a square monolithic honeycomb structure of 400 cells per square inch (cpsi). The thin ceramic walls are coated with a NOx storage/reduction catalyst. The catalytic coating was characterized by X-ray fluorescence analysis (XRF), X-ray diffraction (XRD), scanning electron microscopy with elemental analysis by energy-dispersive X-ray spectroscopy (SEM-EDX). TEM observations were performed on a JEOL 2100F 200 kV microscope equipped with a X-ray dispersive Spectrometer. X-ray diffraction (XRD) patterns were obtained with a PANalytical X'Pert Pro MPD Diffractometer with Bragg-Brentano X-ray tube Cu anticathode (wavenumber kA1 = 1.5406 Å). Samples were loosely packed in a shallow cavity (0.2 cm deep and 1 cm in diameter). The washcoat was separated from the cordierite support before being analysed.

2.2. Aged catalysts

NOx trap samples were hydrothermally aged in a furnace at 800 °C for 5 h under a flow of 10% O_2, 10% H_2O and N_2.

The vehicle aged trap underwent an accelerated aging of 35,000 km with a 10 ppmS fuel, which was equivalent to a mileage of 80,000 km. The catalyst underwent a total of 4 h of desulfation, with a maximum temperature of 780 °C.

2.3. IR operando measurements

The purpose of FTIR Operando study was to analyse NOx and carbonates storage sites of the LNT samples under representative running conditions so as to determine the impact of thermal aging on the storage sites. The description of the Operando setup, with gas line and analysis tools (IR, MS and chemiluminescence) and the IR reactor cell is described in [13]. The material was pressed into self-supporting wafers of 10 mg cm^{-2} and placed into the quartz reactor equipped with KBr windows. For the analysis of the surface, operando measurements were carried out with a Nicolet FT-IR Nexus spectrometer equipped with a MCT detector, using a setup described in [13]. FT-IR spectra were collected with a resolution of 4 cm^{-1}. The analysis of the outlet gases was performed by means of a Pfeiffer Omnistar mass spectrometer. Likewise FT-IR spectra of the gas phase were collected using a gas microcell. The sample was activated in the same way as SGB (described in Section 2.4).

The lean reacting gas composition was 900 ppmC HC, 800 ppm CO, 270 ppm H_2, 300 ppm NOx, 5% CO_2, 15% O_2 and 2% H_2O in Ar as carrier gas. The total flow was fixed to 25 cm^3 min^{-1}. This composition is equivalent to that used in the synthetic gas bench and is very similar to a real composition of a typical Diesel exhaust. Binary mixtures were also used to improve the understanding of NOx storage mechanisms.

2.4. Synthetic gas bench

The purpose of the synthetic gas bench study was to quantify NOx storage and reduction capacities of the LNT samples under representative running conditions so as to evaluate the impact of thermal aging. The following experiments were performed:

- sample pre-treatment
- isothermal NOx storage experiments with different gas compositions
- rich pulses to mimic storage/reduction cycles occurring in real driving conditions

Table 1
Gas compositions used for the tests. Gas composition also included H_2 = CO/3, H_2O = 4% and N_2 = balance.

Eq. ratio	HC (ppmC)	CO	NO (ppm)	CO_2 (%)	O_2 (%)
0.3	900	800	300	5	15
1.1	4500	4%	0	11	1.5

LNT samples prepared for the SGB study were cylinders 25 mm in diameter and 50 mm in length cut from the monolith. Experiments were carried out in a flow reactor under atmospheric pressure and realistic flow conditions with a simulated Diesel exhaust gas stream. The catalyst sample was placed in a quartz tube. A thermocouple in front of the catalyst was used to control the temperature and another one was inserted downstream from the catalyst. The quartz tube was placed in an electrically heated oven. Valves allowed to rapidly switch from one gas composition to another, and to generate alternating rich and lean phases. Gas compositions were chosen close to a lean Diesel environment [equivalence (Eq.) ratio = 0.3] and to a rich pulse environment (Eq. ratio = 1.1) as detailed in Table 1. Other compositions were also tested when considered useful to better understand the catalyst behaviour. Propylene was used to represent unburned hydrocarbons emitted by engine combustion.

The gas hourly space velocity was 30,000 h^{-1}. All gases were fed to the reactor via mass flow controllers, while water vapor was injected through a vaporizer in a N_2 flow. Analysed gases were CO_2, O_2, CO, HC, NOx, NO and NO_2, N_2O and NH_3 for some of the tests.

2.4.1. Sample pre-treatment

All samples were pre-treated to stabilize their active surface and thus their catalytic activity so as to ensure a good test reproducibility. The gas flow was switched between 290 s lean feed periods (Eq. ratio = 0.3) and 15 s rich pulses (Eq. ratio = 1.1, see Table 1). Temperature was increased at 5 °C/min rate from 50 °C up to 620 °C and then stabilized at 620 °C for 2 h. The catalyst was cooled back to room temperature in a synthetic air flow.

2.4.2. Isothermal NOx storage

The gas temperature was increased up to the desired value under a N_2 flow. The experiment then switched to a lean feed and both NO and NO_2 were monitored downstream from the catalyst. The gas mixture switched back to N_2 after the NOx trap became saturated and the temperature was increased so as to thermally release the complete amount of stored NOx (N_2-TPD: temperature programmed desorption). The NOx storage capacity (NSC), the NO oxidation efficiency and the deNOx of the LNT were determined at different temperatures and storage times.

2.4.3. Lean–rich cycling conditions

The method to evaluate NOx storage, reduction and global conversion efficiency of the NOx trap is by cycling between lean and rich conditions to mimic engine operation. In this test, the gas temperature was increased up to the desired value (300 °C) under a N_2 flow. The gas flow was then switched between 290 s lean feed periods (Eq. ratio = 0.3) and 15 s rich pulses (Eq. ratio = 1.1). It was switched back to N_2 after the lean/rich cycling exhibited a repeatable behaviour, and a temperature programmed desorption was performed. The NOx storage efficiency in the lean phase, the NOx reduction efficiency in the rich phase and the overall NOx conversion efficiency were determined as described below.

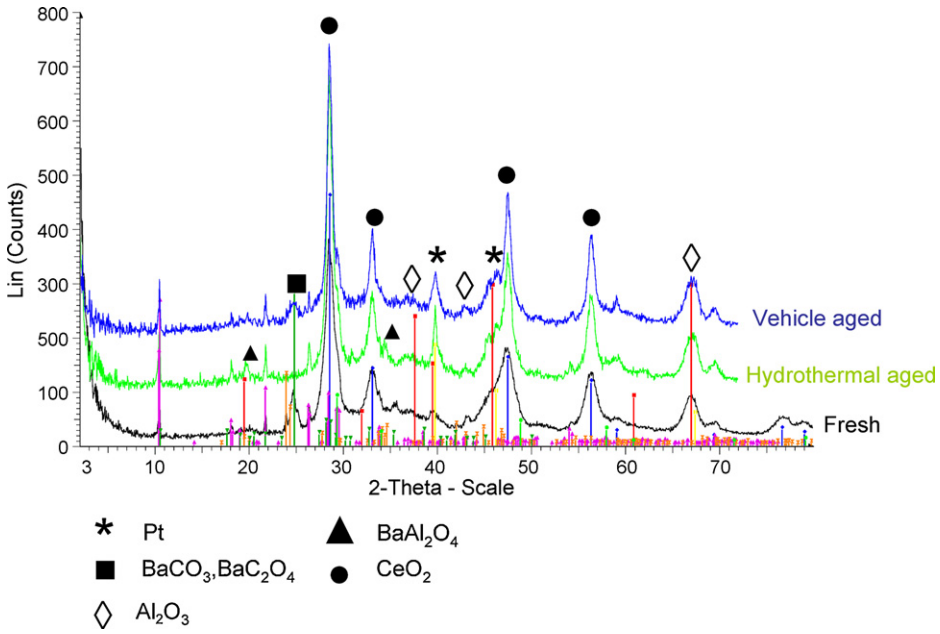

Fig. 1. XRD patterns of fresh LNT, thermal and vehicle aged LNT's. The main peaks are assigned to crystalline phases as indicated.

The NOx storage efficiency represents the proportion of NOx stored in the trap during the lean phase:

$$\eta_{\text{storage NOx}}(\%) = \left(1 - \frac{\int_{t0}^{t1} \text{NOx}_{\text{out}}}{\int_{t0}^{t1} \text{NOx}_{\text{sat}}}\right) \times 100$$

where the lean phase starts at time $t0$ and ends at time $t1$, NOx_{out} are NOx mesured downstream from the NOx trap, and NOx_{sat} is the level of NOx that would be reached if the lean phase is long enough to saturate the trap. NOx_{sat} can also be determined from the amount of N_2O emitted because the DeNOx is completely non-selective in our lean conditions.

The NOx reduction efficiency is determined during the rich phase:

$$\eta_{\text{red NOx}}(\%) = \left(1 - \frac{\int_{t1}^{t2} \text{NOx}_{\text{out}}}{\int_{t1}^{t2} \text{NOx}_{\text{in}} + \text{NOx}_{\text{stored}}}\right) \times 100$$

where the rich phase starts at time $t1$ and ends at time $t2$, NOx_{in} are NOx mesured upstream of the NOx trap, and $\text{NOx}_{\text{stored}}$ is the quantity of NOx that were stored during the lean phase:

$$\text{NOx}_{\text{stored}} = \int_{t0}^{t1} \text{NOx}_{\text{sat}} - \text{NOx}_{\text{out}}$$

The overall NOx conversion efficiency is determined during the two phases.

$$\eta_{\text{conv NOx}}(\%) = \left(1 - \frac{\int_{t0}^{t2} \text{NOx}_{\text{out}}}{\int_{t0}^{t2} \text{NOx}_{\text{in}}}\right) \times 100$$

3. Results and discussion

3.1. Catalyst composition and characterisation

According to XRF composition analysis, main components of the washcoat are Al_2O_3, ZrO_2 and CeO_2. Trapping materials are mainly Ba and Sr. Active species are Pt and Rh. A combination of these two noble metals is required to achieve good NOx storage and reduction performance, together with good sulphur regeneration ability [14]. SEM reveals that the washcoat is deposited into the pores and hence intimately bound to the cordierite support, and also that Pt and Ba are close to each other (SEM-EDX). Fig. 1 displays XRD spectra of the fresh, thermal and vehicle aged catalysts. For thermal and vehicle aged catalysts, the Pt peak at $2\theta = 40^\circ$ sharpens with aging temperature, indicating that Pt particle sintering increases [15]. Other authors, using in situ XRD, have previously shown [16] that metallic Pt particles in a simple model $Pt/BaO/Al_2O_3$ LNT exponentially grow with increasing treatment temperatures above 700 °C under a lean gas mixture similar to that used here. TEM results on Pt coarsening are in agreement with those obtained by XRD. BET surface areas of aged catalysts decreased accordingly (Table 2).

In the fresh catalyst, $BaCO_3$ and BaC_2O_4 are the predominant Ba-phases observed in the XRD pattern. Hydrothermal aging at 800 °C makes the Ba-phase react in solid phase with γ-Al_2O_3 and leads to $BaAl_2O_4$ as can be seen at $2\theta = 20^\circ$. In the vehicle aged catalyst $BaCO_3$ and BaC_2O_4 diminish compared to the fresh sample as can be seen at $2\theta = 25^\circ$. XRD analysis does not detect $BaAl_2O_4$ nor $BaSO_4$ crystal formation. XRF analysis of the vehicle-aged catalyst allows to identify the residual sulphur (0.5 g/l left uniformly). This one comes from both fuel and lubricant. According to SEM-EDX, the residual sulphur is associated with Ba. This contributes to the reduction of the NOx storage sites [17]. The alumina peak at $2\theta = 67.5^\circ$ indicates γ-Al_2O_3 (cubic structure). This alumina phase remains unchanged in all cases.

3.2. Surface characterisation by Operando FTIR

The NOx storage properties of the samples were evaluated by *Operando* FTIR during isothermal NOx storage exper-

Table 2
BET surface areas of fresh and aged catalysts.

Catalysts	Surface area (m^2/g)
Fresh	139
Hydrothermal aged (HA) 800 °C	98
vehicle-aged (VA)	95

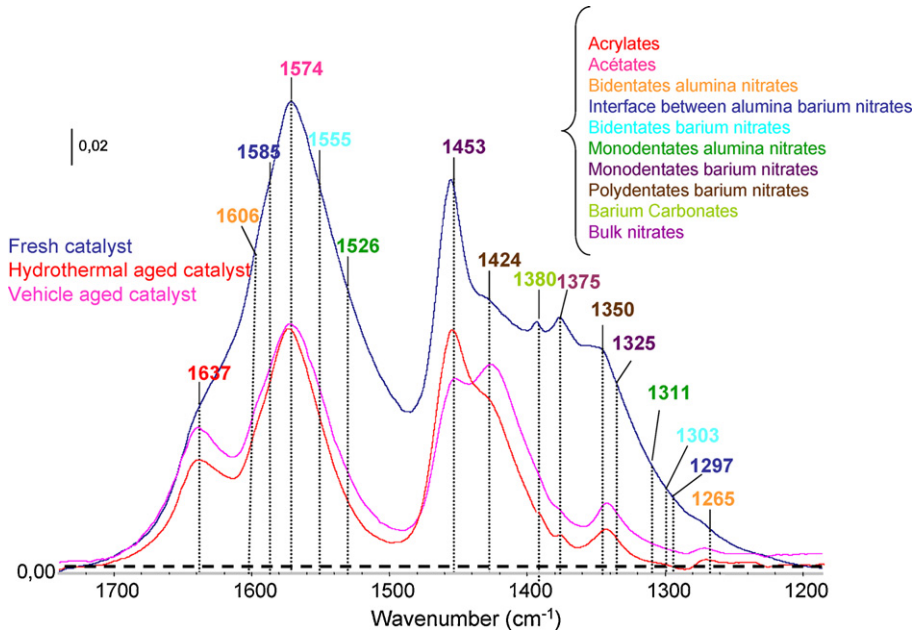

Fig. 2. IR surface spectra at 200 °C of the fresh, hydrothermally (800 °C) and vehicle aged NOx-trap after exposure to a lean flow (Eq. ratio = 0.3). Some of the peaks are unresolved.

iments under realistic conditions. Fig. 2 shows the spectra of the nitrate and carbonate species on the surface of fresh, vehicle and hydrothermal aged (800 °C) catalysts once saturated.

The graph shows competition between nitrate, carbonate and hydrocarbon species, giving rise to a complex massif. However acrylates coordinated with Al_2O_3 (1637 and 1424 cm^{-1}), acetates (1574 and 1454 cm^{-1}) and carbonates (1380 cm^{-1}) [18] can be distinguished. A test in a flow containing $NO + O_2$ was done to help us to assign nitrate species (results not displayed). We can distinguish the formation of bidentate nitrates coordinated with alumina cations (bands at 1606–1265 cm^{-1}) [19,20]. We can also distinguish the formation of bidentate nitrates coordinated at the interface between alumina and barium oxide (bands at 1585 and 1297 cm^{-1}) [21], bidentate nitrates coordinated with Ba^{2+} cations (1555 and 1303 cm^{-1}) [22], monodentate nitrates coordinated with Al_2O_3 (1526 and 1311 cm^{-1}) [19], monodentate nitrates coordinated with Ba^{2+} cations (1453 and 1325 cm^{-1}) [23,24], polydentate nitrates coordinated with Ba^{2+} cations (1426 and 1350 cm^{-1}) [25] and bulk nitrates [18], according to their wavenumber (1375 cm^{-1}).

Compared to the fresh catalyst, nitrate, carbonate and hydrocarbon species remain the same after aging. The two aging processes lead to the same FTIR spectrum with similar band intensities for all species. Furthermore, mass spectrometry showed that the quantity of NOx stored was the same (results not displayed).

During the FTIR Operando test performed under $NO + O_2$ flow (Ar as carrier gas), ionic nitrites were detected with a band intensity that was greater at 200 °C than 300 °C (results not displayed) [26,27]. The presence of these ionic nitrites may indicate that NO_2 oxidation into NO_3 on the storage sites becomes a limiting step in NOx storage at 200 °C.

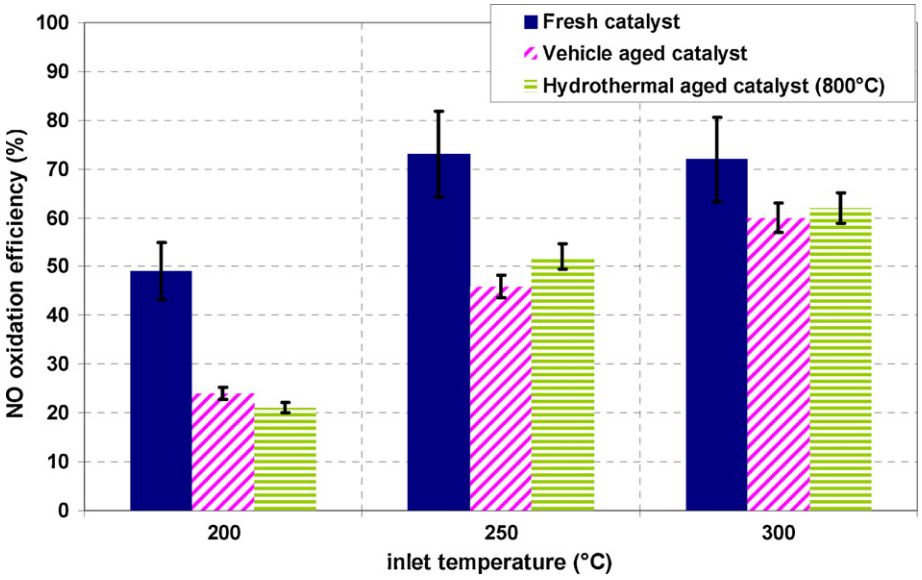

Fig. 3. Synthetic gas bench measurements of NO oxidation efficiency of the fresh and aged LNTs (Eq. ratio = 0.3).

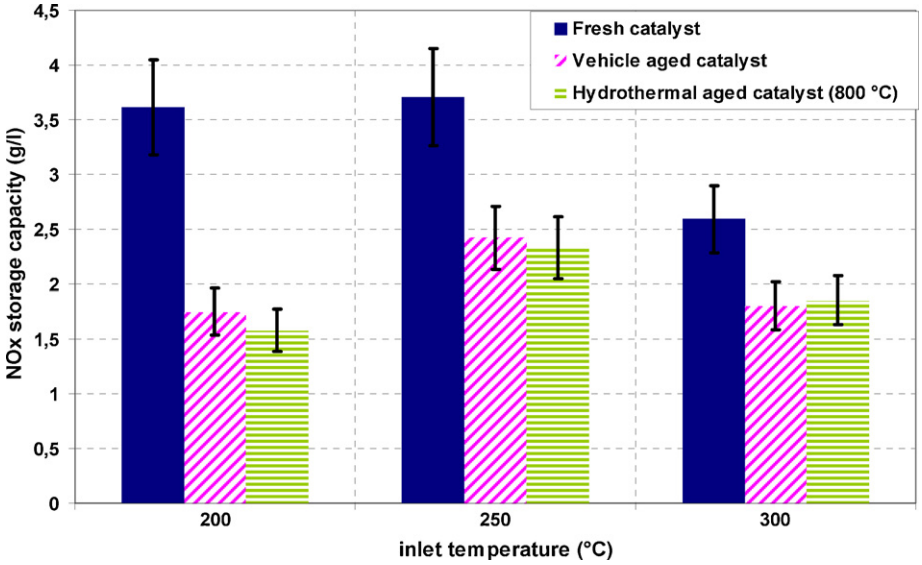

Fig. 4. Synthetic gas bench measurements of NOx storage capacity of the fresh and aged LNTs (Eq. ratio = 0.3).

3.3. *Isothermal NOx storage on the synthetic gas bench*

Fig. 3 shows the NO oxidation efficiency of fresh, hydrothermally and vehicle aged catalysts as a function of the inlet gas temperature (200, 250 and 300 °C).

Hydrothermal and vehicle aging processes both lead to a similar loss of NO oxidation efficiency which is more significant at 200 °C than at 300 °C. This is due to Pt sintering that reduces the number of sites available to oxidize NO to NO_2. NO oxidation efficiency decreases by about 60% between the fresh and the aged samples at 200 °C. NO_2 formation is kinetically controlled at this temperature and is hence strongly sensitive to Pt sintering, as was demonstrated by Takahashi et al. [1]. The impact weakens at 300 °C and above when the thermodynamical equilibrium between NO and NO_2 becomes dominant: the NO oxidation efficiency only decreases by 17% between the fresh and the aged samples. Despite a greater sintering of Pt on the hydrothermal aged catalyst, the impact on NO oxidation is similar on both aged catalysts.

Fig. 4 shows the NOx storage capacity of fresh and aged catalysts as a function of the inlet gas temperature (200, 250 and 300 °C). In agreement with *Operando* FTIR results (Figure 2), hydrothermal and vehicle aging processes lead to a similar NOx storage capacity decrease, with again a stronger impact at 200 °C (−55%). This was expected since it partly depends on the NO oxidation efficiency of the sample, as one effective pathway for NOx storage from NO/O_2 mixtures is the "nitrite" route, which implies the stepwise oxidation of NO leading to the formation of nitrite ad-species [28–31].

The NOx storage capacity also depends on the storage material performance [2,32]. A specific isothermal NOx storage test was performed to better distinguish the impact of the storage material from the oxidation parameter on Pt sites on the aged samples. A simple flow of 300 ppm NO_2 in nitrogen was used in order to bypass the NO oxidation step. This experiment was performed on the fresh and aged NOx trap samples, in a temperature range where NO_2 formation is kinetically controlled, i.e. far from thermodynamic equilibrium. Results are displayed in Fig. 5 and show that the NOx storage capacity still decreases by up to 30%. The reduction of NOx storage capacity is similar on both aged catalysts, although it may be due to various reasons.

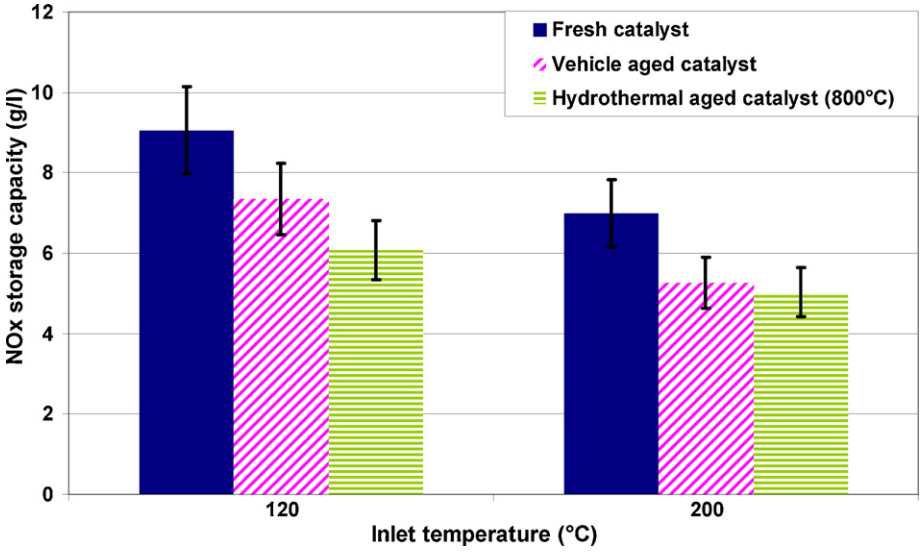

Fig. 5. Synthetic gas bench measurements of NOx storage capacity in the fresh and aged LNTs (300 ppm NO_2 in N_2).

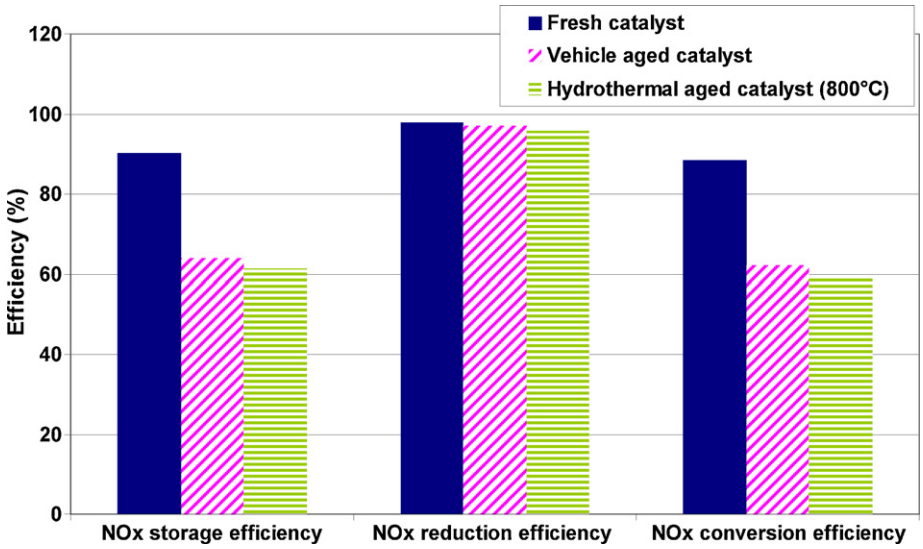

Fig. 6. Synthetic gas bench measurements of NOx storage, NOx reduction and NOx conversion efficiencies during NOx storage/reduction cycles on fresh aged LNTs – inlet gas temperature = 300 °C (Eq. ratio = 0.3/1.1).

These tests indicate that different factors are responsible for NSC reduction due to aging. The proximity of platinum and barium is important since Pt helps to store NOx in the trap, as a large Pt/BaO interfacial perimeter enhances the spillover of NOx between the precious metal and storage component [33–35]. By decreasing the number of Pt–Ba neighbouring couples, Pt sintering shrinks the Pt/Ba interface and may hence be partly responsible for this decrease, apart from its impact on NO oxidation. The storage site reduction of the hydrothermal aged catalyst is also attributed to the conversion of $BaCO_3$ and BaC_2O_4 storage sites to $BaAl_2O_4$ as was highlighted by XRD patterns (Fig. 1). On the other hand, barium storage sites are still available in the vehicle aged catalyst according to XRD analysis, but SEM-EDX detected the presence of sulphur trapped on barium. XRF determined a 0.5 g/l sulphate amount. With the assumption that it is all coordinated to barium under the form of $BaSO_4$, this represents poisoning of 20% of barium and/or strontium sites available for NOx storage if compared to the NSC of the fresh catalyst (3.7 g/l of NO_2 stored at 250 °C as $Ba(NO_3)_2$, see Fig. 4).

3.4. Lean–rich cycling conditions

The impact of thermal and vehicle aging was also investigated in conditions close to real use, i.e. by periodically switching the gas composition between 290 s lean feed periods and 15 s rich pulses to regenerate the NOx trap. Results are summarized in Fig. 6 at 300 °C inlet gas temperature.In agreement with isothermal NOx storage test results, the NOx storage efficiency determined during NOx storage/reduction cycles was reduced in similar proportions by both aging processes: from 90% for the fresh sample down to 60% for the aged samples. On the other hand, for this test conditions, the NOx reduction efficiency during rich pulses remains constant and close to 100% for all samples. Therefore, the decrease of the global NOx conversion efficiency is mainly due to the NOx storage efficiency lowering. It also appears that the rich pulse duration was not sufficient anymore to ensure complete NOx-trap regeneration: an amount of NOx (around 8% of the NSC) remained stored in the aged traps. This might be due to a greater proportion of bulk Ba storage sites leading to more stable nitrates. Another possible reason is Pt sintering and its effect on the Pt/Ba interface: as demonstrated by Rodriguez [33], the proximity of platinum and barium is important since Pt helps to remove and reduce NOx from the trap.

4. Conclusions

This study showed that synthetic gas bench (SGB), *Operando* FTIR, SEM-EDX and XRD are useful and complementary techniques to characterise the effect of aging on a commercial lean NOx-trap. Two aging processes were tested: a hydrothermal aging at 800 °C and a vehicle aging corresponding to 80,000 km use. They had a similar impact on the LNT functionalities; and the reduction of the global NOx conversion efficiency by about 30% appeared to be the consequence of a drop in the NOx storage capacity. These changes were however due to different structural evolutions depending on the aging process:

- Common evolutions: Pt sintering was greater after thermal aging than after vehicle aging despite similar impact on the NO oxidation functionality. It also changed the Pt/Ba interface and may hence be partly responsible for the NSC decrease.
- LNT structural evolutions specific to hydrothermal aging: $BaCO_3$ and BaC_2O_4 conversion to $BaAl_2O_4$ which further decreases the number of available storage sites.
- LNT structural evolutions specific to vehicle aging: no $BaAl_2O_4$ formation was observed but barium storage sites were poisoned by residual sulphur which also further decreases the number of available storage sites.

Although the reduction efficiency was scarcely affected, an amount of NOx (8% of the NSC) remained stored in the trap. Regenerations appeared to be less efficient, which was attributed to a slower NOx release during rich pulses. The Pt/Ba interface change after Pt sintering could also partly explain this results.

Acknowledgments

The authors wish to thank the analysis department (XRD, TEM, XF, etc.) at IFP Energies nouvelles for the help during the study. ANRT support for S. Benramdhane PhD. grant is also gratefully acknowledged as well as Renault for supplying the catalysts.

References

[1] N. Takahashi, H. Shinjoh, T. Iijima, T. Suzuki, K. Yamazaki, K. Yokota, H. Suzuki, N. Miyoshi, S. Matsumoto, T. Tanizawa, T. Tanaka, S. Tateishi, K. Kasahara, Catal. Today 27 (1996) 63.

[2] L. Gill, P. Blakeman, M. Twigg, A. Walker, Top. Catal. 28 (2004) 157.
[3] R. Burch, T.C. Watling, Appl. Catal. B 17 (1998) 131.
[4] P. Engström, A. Amberntsson, M. Skoglundh, E. Fridell, G. Smedler, Appl. Catal. B-Environ. 22 (1999) L241.
[5] A. Amberntsson, B. Westerberg, P. Engström, E. Fridell, M. Skoglundh, B. Delmon, G.F. Froment, Stud. Surf. Sci. Catal. 126 (1999) 317.
[6] H. Mahzoul, L. Limousy, J.F. Brilhac, P. Gilot, J. Anal. Appl. Pyrol. 56 (2000) 179.
[7] S. Matsumoto, CATTECH 4 (2000) 102.
[8] F. Rohr, S.D. Peter, E. Lox, M. Kögel, A. Sassi, L. Juste, C. Rigaudeau, G. Belot, P. Gélin, M. Primet, Appl. Catal. B-Environ. 56 (2005) 201.
[9] C. Courson, A. Khalfi, H. Mahzoul, S. Hodjati, N. Moral, A. Kiennemann, P. Gilot, Catal. Commun. 3 (2002) 471.
[10] S. Elbouazzaoui, X. Courtois, P. Marecot, D. Duprez, Top. Catal. 30/31 (2004) 493.
[11] N. Fekete, J. Leyrer, R. Kemmler, B. Krutzsch, G. Wenninger, SAE International Technical Papers, 970746, 1997.
[12] B.-H. Jang, T.-H. Yeon, H.-S. Han, Y.-K. Park, J.-E. Yie, Catal. Lett. 77 (2001) 21.
[13] T. Lesage, C. Verrier, P. Bazin, J. Saussey, M. Daturi, Phys. Chem. Chem. Phys. 20 (2003) 4435.
[14] A. Amberntsson, E. Fridell, M. Skoglundh, Appl. Catal. B-Environ. 46 (2003) 429.
[15] G.W. Graham, H.-W. Jen, W. Chun, H.P. Sun, X.Q. Pan, R.W. McCabe, Catal. Lett. 93 (2004) 129.
[16] D.H. Kim, Y.H. Chin, G. Muntean, A. Yezerets, N.W. Currier, W.S. Epling, H.Y. Chen, H. Hess, H.F. Peden, Ind. Eng. Chem. Res. 45 (2006) 8815.
[17] C. Sedlmair, K. Seshan, A. Jentys, J.A. Lercher, J. Catal. 214 (2003) 308.
[18] K.I. Hadjiivanov, Catal. Rev. Sci. Eng. 42 (2000) 71.
[19] Westerberg, E. Fridell, J. Mol. Catal. A: Chem. 165 (2001) 249.
[20] J.M. Coronado, J.A. Anderson, J. Mol. Catal. A 138 (1999) 83.
[21] T. Lesage, C. Verrier, P. Bazin, J. Saussey, M. Daturi, Phys. Chem. Chem. Phys. 5 (2003) 4435.
[22] T. Szailer, J.H. Kwak, D.H. Kim, J. Szanyi, C. Wang, C.H.F. Peden, Catal. Today 114 (2006) 86.
[23] H. Abdulhamid, J. Dawody, E. Fridell, M. Skoglundh, J. Catal. 244 (2006) 169.
[24] P.T. Fanson, M.R. Horton, W.N. Delgass, J. Lauterbach, Appl. Catal. B-Environ. 46 (2003) 393.
[25] V.G. Milt, C.A. Querini, E.E. Miró, M.A. Ulla, J. Catal. 220 (2003) 424.
[26] D.H. Kim, J.H. Kwak, J. Szanyi, S.D. Burton, C.H.F. Peden, Appl. Catal. B-Environ. 72 (2007) 233.
[27] Y. Su, M.D. Amiridis, Catal. Today 96 (2004) 31–41.
[28] I. Nova, L. Castoldi, F. Prinetto, V. Dal Santo, L. Lietti, E. Tronconi, P. Forzatti, G. Ghiotti, R. Psaro, S. Recchia, Top. Catal. 30/31 (2004) 181.
[29] F. Frola, F. Prinetto, G. Ghiotti, L. Castoldi, I. Nova, L. Lietti, P. Forzatti, Catal. Today 126 (2007) 81.
[30] P. Broqvist, H. Gronbeck, R. Fridell, I. Panas, Catal. Today 96 (2004) 71.
[31] T. Lesage, J. Saussey, S. Malo, M. Hervieu, C. Hedouin, G. Blanchard, M. Daturi, Appl. Catal. B-Environ. 72 (2007) 166.
[32] M. Takeuchi, S. Matsumoto, Top. Catal. 28 (2004) 1.
[33] F. Rodriguez, PhD, University of Pierre et Marie Curie, Paris VI, October 2001.
[34] P. Forzatti, L. Castoldi, I. Nova, L. Lietti, E. Tronconi, Catal. Today 117 (2006) 316.
[35] R.D. Clayton, M.P. Harold, V. Balakotaiah, C.Z. Wan, Appl. Catal. B-Environ. 90 (2009) 662.